CHAPTER V

MOTOR OIL REMOVAL FROM WASTEWATER BY CONTINUOUS FROTH FLOTATION USING EXTENDED SURFACTANT: EFFECTS OF OPERATIONAL PARAMETERS AND AIR BUBBLE SIZE

5.1 Abstract

The objective of this study was to investigate the bubble characteristics and interfacial area of bubbles in flotation column and the efficiency of motor oil removal from the water under microemulsion conditions by continuous froth flotation. $C_{14\text{-}15}(PO)_5SO_4Na$ (branched alcohol propoxylate sulfate, sodium salt) was used as a surfactant to form a Winsor's type III microemulsion with motor oil. The effects of surfactant concentration and NaCl concentration, where the minimum surfactant concentration can form the Winsor's type III microemulsion, or critical microemulsion concentration (CμC), were studied. After that, the continuous froth flotation experiments were performed to investigate the efficiency of motor oil removal using $C_{14\text{-}15}(PO)_5SO_4Na$ under microemulsion conditions. The effects of surfactant concentration and hydraulic retention time (HRT) on the oil removal were investigated. Froth production rate was found to be a crucial parameter affecting the froth flotation efficiency. Bubble size distribution and bubble axial velocity were also measured in order to correlate with the performance of the froth flotation process.

Keywords: Bubble size distribution, Continuous froth flotation, Microemulsion, Motor oil removal

5.2 Introduction

Motor oil is widely used for lubrication all moving parts, especially internal combustion engines. It also functions to carry heat away from the moving engine parts, as well as to clean and protect the internal surface. Most machines in industrial processes such as compressors, pumps and turbines require motor oil as a lubricant to cover all moving surfaces, and to reduce the friction, and wear between them (1). As

a result, motor oil is often found to present in industrial wastewaters which can affect the performance of wastewater treatment plants. This is because motor oil cannot be degraded biologically. It must be removed prior to entering an existing biological treatment plant.

Froth flotation is a surfactant-based separation process (2-4). It was first used in ore processing, and it has been pointed out to be a promising technique for oily wastewater treatment (3-12). Froth flotation process is suitable for treating wastewater containing suspended solids as well as oils in both emulsion and dissolved forms since it has several advantages, including rapid operation, low space requirement for equipment set-up, high removal efficiency, flexibility of the application to various pollutants at varying scales, and low operating cost (13).

In a froth flotation operation, a proper type and concentration of a surfactant is first added to oily wastewater, and air is introduced into the system in order to generate fine bubbles. The surfactant added tends to adsorb preferentially at the air/water interface with the hydrophilic part or head groups in the water and the hydrophobic part or tail groups in the air. As a result, oil concentrates at the bubble surfaces while they rise through the solution to form foam or froth at the top of the flotation cell, which is continuously skimmed off. The formation of stable bubble particle aggregates is required in the froth flotation operation in order to achieve high separation efficiency (14).

From previous work (7), the maximum removal of orthodichlorobenzene was found to correspond to the ultralow interfacial tension (IFT) condition when the system is in the Winsor's type III microemulsion region. This is the initial point of our research group to continue studying the relationship between the Winsor's type III microemulsion and the froth flotation efficiency with different types of oils because a microemulsion has superior characteristics such as relatively large interfacial area, high solubilization capacity, and ultralow IFT (15). Later, Chavadej *et al.* (8) found that the most orthodichlorobenzene removed during the froth flotation operation came from the excess oil phase rather than from the middle phase in the Winsor's type III microemulsion system. This proves that it is the ultralow IFT corresponding to the presence of a Winsor's type III microemulsion which is responsible for efficient flotation; the formation of a third phase (middle phase)

under this condition is coincidental to high oil removal. Yanatatsaneejit *et al.* (9) found that ethylbenzene removal from water by froth flotation was efficient only when both low IFT and good frothing were present. The importance of froth stability was also observed by Carre *et al.* (16). Moreover, Yanatatsaneejit *et al.* (10) proposed four sequential steps in the mechanism of oil removal by froth flotation. Firstly, air bubbles are generated through the liquid solution, and oil droplets adhere to the surface of the air bubbles. The second step is the formation of oil films on the surfaces of the air bubbles while the air bubbles are rising through the solution. The third step is the rising of the air bubbles with attached oil films to the top of the solution. The fourth step is the emergence of the air bubbles from the liquid phase to form froth. In both the third and fourth steps, high stability of the oil-film covered air bubbles is necessary. For successful separation, high stability of the froth is needed in order to yield dry froth with high oil content. Froth formation and froth stability influence the froth production rate, which needs to be sufficient for good separation, no matter how well the oil attaches to the air bubbles rising through the solution. Yanatatsaneejit *et al.* (11) correlated the performance of batch froth flotation to remove diesel oil from water with the system IFT, froth characteristics, and coalescence time between oil droplets. The results indicated that both IFT and froth characteristics had to be optimized to achieve a high efficiency of oil removal in a froth flotation operation. However, the coalescence time between oil droplets was not a significant parameter for a successful froth flotation operation. In addition, Watcharasing *et al.* (12) firstly investigated oily wastewater treatment by a continuous froth flotation operation. A branched alocohol propoxylate sulfate, sodium salt ($C_{14\text{-}15}(PO)_5SO_4Na$), an extended surfactant was used to form microemulsions with diesel oil in this study. The fish diagram which is plotted between microemulsion type and surfactant concentration was constructed to determine the critical microemulsion concentration (CμC), the lowest surfactant concentration to form a Winsor's type III microemulsion. The obtained value of the CμC was then selected as a base condition to run the continuous froth flotation experiments. Unlike the batch mode of operation, the $C_{14\text{-}15}(PO)_5SO_4Na$ system alone was not able to generate stable froth for the continuous froth flotation

operation. Hence, sodium dodecyl sulfate (SDS) was added as a froth booster. It was concluded that not only the low IFT, but also froth formation and froth stability were needed for high oil removal in the froth flotation operation.

The presence of a gas phase dispersed in a continuous liquid in the froth flotation column plays a significant role in influencing the mass transfer surface area. Small bubbles and a homogeneous gas distribution throughout the column are desired to maximize the mass-transfer interfacial area of the system (17, 18). The bubble size distribution in the froth flotation column can be used to determine the mass transfer interfacial area (19). The interfacial adsorption of surfactants is a crucial mechanism step, causing the reduction of surface tension which correlates with the frother behaviour in the flotation process performance (20). However, in many interfacial processes, such as foaming, equilibrium conditions are not attained and dynamic IFT plays a major role affecting the process performance (21). The importance of such dynamic IFT is pointed out to be essential for deeply understanding of interfacial processes including froth flotation. Moreover, the bubble rising velocity and, consequently, the average residence time of air bubbles have to be considered for operation and design of a froth flotation unit (22, 23).

In this work, the relationship between the bubble characteristics and interfacial surface area of air bubbles in the froth flotation column and the efficiency of motor oil removal from water under microemulsion conditions by continuous froth flotation was investigated. $C_{14\text{-}15}(PO)_5SO_4Na$ (branched alcohol propoxylate sulfate, sodium salt) was used to form microemulsions with motor oil. The effects of surfactant concentration and NaCl concentration were studied in the microemulsion phase study in order to determine the minimum surfactant concentration to form a Winsor's type III microemulsion, or critical microemulsion concentration (CμC). Next, the continuous froth flotation experiments were performed to investigate the efficiency of motor oil removal from water at different surfactant concentrations and hydraulic retention times (HRT). Moreover, bubble size distribution and bubble axial velocity were also measured in order to correlate with the performance of the froth flotation process.

5.3 Experimental Section

5.3.1 Materials

A branched alcohol propoxylate sulfate, sodium salt ($C_{14\text{-}15}(PO)_5SO_4$) with 28.7% active in liquid form was supplied by Sasol North America Inc., Texas, USA. It is an extended anionic surfactant having 14-15 carbon atoms and 5 groups of propylene oxide (PO) with sulfate as the hydrophilic group. Motor oil was selected a model contaminant oil which is commercially available for use in gasoline engines, type SAE 10W-30 with synthetic guard (Castrol GTX). It consists of a base lubricating oil (a complex mixture of hydrocarbons, 80 to 90% by volume) and performance enhancing additives (10 to 20% by volume) (24). Analytical grade sodium chloride (NaCl) with 99% purity was obtained from Labscan Asia Co., Ltd. All chemicals were used as received without further purification. Deionized water was used to prepare all aqueous solutions.

5.3.2 Methods

This work was divided into five main parts. The first part was a study of microemulsion formation of motor oil with aqueous solutions of varying surfactant and NaCl concentrations. The second part was a dynamic surface tension measurement. For the third part, continuous froth flotation experiments were conducted at various surfactant concentrations and hydraulic retention times (HRT). The fourth part was a study of air bubble size distribution in the froth flotation column. The final part was froth characteristics experiments.

5.3.2.1 Microemulsion Formation Studies

A quantity of 5 ml of motor oil was added to a series of vials containing 5 ml of a surfactant solution having different surfactant concentrations and salinities. After that, each vial was shaken gently by hand for 1 min and then equilibrated in a temperature-controlled incubator (Binder, KB400/E2) for 4 weeks at 30°C. The equilibrium state was considered to be attained when the volume of each phase of the microemulsion system was invariant. The measurement of phase height was conducted by using a cathetometer, model TC-II from Titan Tool Supply, Inc.,

attached to a digimatic height gauge, model 192-631, from Mituyo, with ± 0.002 mm accuracy. The IFT between the motor oil and the various surfactant solutions was measured using a spinning drop tensiometer (Krüss, SITE 04).

At a very low surfactant concentration, it was difficult to visually observe which microemulsion type was present since the phase volume of any middle phase formed was so small. Therefore, electrolytic conductivity was used to determine the microemulsion type instead (25, 26). For each condition, the electrolytic conductivity was measured, under gentle stirring with a magnetic stirrer, by using a conductivity meter (Eutech Instruments, CON11&CON110) at room temperature (26±1°C). Since the aqueous phase contained a certain concentration of sodium chloride, the inversion was easily monitored by a change of two or more orders of magnitude in conductivity (mS/cm or μS/cm) (25). High conductivity indicates a Winsor's type I or III microemulsion while a low value implies a Winsor's type II microemulsion (26). The results obtained from the conductivity and IFT measurements and visual observation were used to plot the microemulsion phase diagram or conditions where Winsor's type I, II and III microemulsions exist. When plotted as surfactant concentration vs. salinity (or vice versa), these phase plots are called fish diagrams. The fish diagrams are generally used to determine a minimum surfactant concentration required to form a Winsor's type III microemulsion which is known as the critical microemulsion concentration (CμC).

5.3.2.2 Dynamic Surface Tension Measurement

Dynamic surface tension was measured by using the maximum bubble pressure method (21, 27). The dynamic surface tension, especially at short periods, corresponding to the age of air bubbles (28), was reportedly an important property for the evaluation of froth flotation process performance (22-23). In this study, dynamic surface tension measurements were carried out using a bubble pressure tensiometer (Krüss, BP2). To operate the bubble pressure tensiometer, a gas bubble was generated using a capillary tube. During this process, the pressure inside the air bubble was monitored and recorded with time until the burst of the air bubble. The maximum rate of decrease in surface tension $(d\gamma_t/dt)_{max}$ is calculated using the

dynamic surface tension data (27). There are four regions of the change in dynamic surface tension with bubble surface lifetime that consists of induction, rapid fall, meso-equilibrium, and equilibrium. The first three regions are important in high speed dynamic processes such as frothing. The dynamic surface tension, γ_t, at a constant surfactant concentration can be expressed by the relaxation function (29):

$$\gamma_t = \gamma_m + (\gamma_0 - \gamma_m)/\{1 + (t/t^*)^x\} \quad [1]$$

where γ_t is the dynamic surface tension at any time, γ_0 is the solvent (water) surface tension, γ_m is the meso-equilibrium surface tension, t is the time that γ_t attained, t* is the time when γ_t attained a half value between γ_0 and γ_m, and x is a constant. The x and t* values are calculated by the curve fitting. The differential form of Eq. [1] becomes

$$\frac{d\gamma_t}{dt} = -\frac{(\gamma_0 - \gamma_m)[x(t/t^*)^{x-1}/t^*]}{[1 + (t/t^*)^x]^2} \quad [2]$$

Then, $(d\gamma_t/dt)_{max}$ is derived from substituting t* for t in Eq.[2] as expressed in Eq. [3].

$$\frac{d\gamma_t}{dt} = \frac{x(\gamma_0 - \gamma_m)}{4t^*} = -(d\gamma_t/dt)_{max} \quad [3]$$

5.3.2.3 Froth Flotation Experiments

Figure 5.1 shows a schematic of the continuous froth flotation unit used in this study. The froth flotation column was made of a glass cylindrical tube with 5 cm inside diameter and 120 cm height, and it was operated in continuous mode. Compressed air was first filtered to remove all particles, water, and oil before entering the froth flotation column. The flow rate of the filtered air was regulated by a mass flow controller (Aalborg, GFC171S). The filtered air was introduced into the bottom of the column through a sinter glass disk with pore diameters of about 16-40 μm. A well-mixed solution, containing 500 ppm motor oil with different

surfactant and NaCl concentrations, was fed continuously at a desired flow rate into the froth flotation column by using a peristaltic pump (Masterflex, Easy-load II). The level of the solution in the column was adjusted by a three-way flexible outlet tube in order to vary the froth height. The air bubbles ascending through the solution in the column generated froth which overflowed from the top of the column and was collected in a froth receiver, and then the collapsed froth was analyzed for motor oil and surfactant concentrations in the froth. In addition, liquid effluent samples were also collected for the analysis of motor oil concentration and surfactant concentration by using the methylene chloride extraction method (31) and the titration method with methylene blue chloride (32), respectively. All froth flotation experiments were carried out at room temperature of 26±1°C. Each experiment was run until the system reached steady state. The steady state was justified when the concentrations of motor oil in the froth and liquid effluent samples became invariant. The reported data obtained under steady state conditions were averaged from at least three samples from each run to evaluate the process performance.

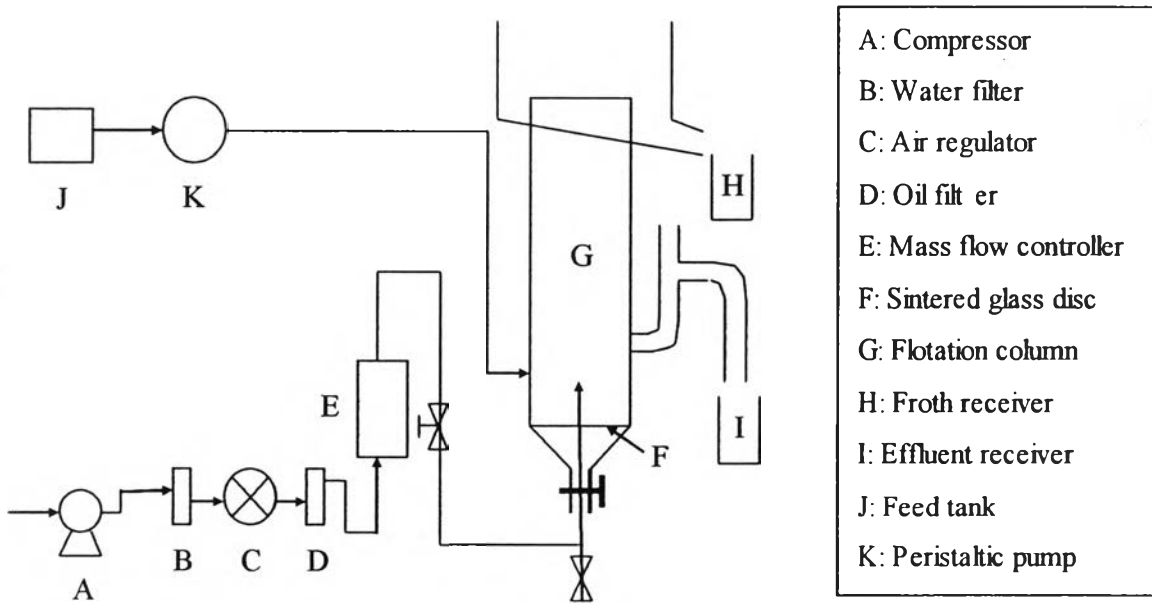

Figure 5.1 Schematic of the froth flotation apparatus with a continuous mode of operation used in this study.

5.3.2.4 Measurement of Air Bubble Size Distribution in Froth Flotation Column

The measurement of the air bubble size distribution in the studied froth flotation column was carried out by photographic method. Images of the air bubbles were taken by using a color video camera (Sony, SSC-DC58AP/1), connected to the optical lens (OPTEM). A light generation unit (Photonic, PL 3000) was used to obtain clear-cut images. The light source with semi-rigid fiber optic light guides and lenses permits the light beam to be directed to any specific position. In order to minimize the effect of the curvature of the froth flotation column on the images taken by the camera, the point on the centerline of the column was used for taking the photographs at three different axial positions along the column for different operating conditions. Figure 5.2 shows typical photographs taken at three different heights. One hundred images were taken at a time interval of 1 s. For obtaining a sufficiently representative bubble size distribution, at least 500 bubbles were fitted and the Image-Pro Plus software (version 5.1) was used to evaluate the diameter of each individual bubble and then both average diameter and diameter size distribution of air bubbles were obtained (30).

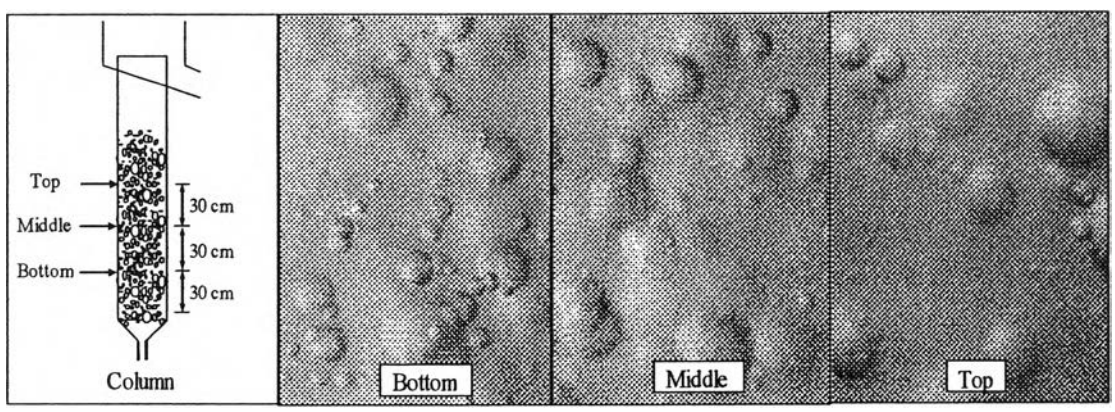

Figure 5.2 Photographs taken from three different heights of the flotation column.

5.3.2.5 Froth Characteristic Experiments

The froth characteristic experiments were independently conducted in a glass cylinder having the same inside diameter as the froth flotation

column. A quantity of 250 ml of the solution sample with motor oil and various surfactant and NaCl concentrations was transferred to the column. After that, filtered air at a constant flow rate of 0.1 L/min was introduced into the bottom of the column through a sintered glass disc to generate fine bubbles through the solution. When, for each run, the maximum froth height was achieved and recorded, the air flow was then terminated. The ratio of maximum froth height to initial solution height is defined as the froth formation while the time required for the froth volume to collapse to half of the maximum froth height is defined as froth stability ($t_{1/2}$). All experiments were carried out at room temperature (26±1°C).

5.4 Results and Discussion

In all experiments, the surfactant and NaCl concentrations are expressed in weight percent (wt.%) per volume of the aqueous phase consisting of water, salt, and surfactants (not including the oil phase).

5.4.1 Phase Behaviors

A low or ultralow oil/water IFT can greatly enhance the performance of froth flotation, as mentioned in our previous studies (7-12). The use of extended surfactants can form microemulsions with a variety of oils without added alcohol at room temperature (33). Hence, $C_{14-15}(PO)_5SO_4Na$ was selected to form micromulsions with motor oil in the present study. It is of interest to know a minimum surfactant concentration required to exhibit a Winsor's type III microemulsion which is known as the critical microemulsion concentration (CμC) (34). This is because under this Winsor's type III microemulsion condition, the system exhibits ultralow IFT, resulting in high oil removal (7). Figure 5.3 shows the relation between conductivity and microemulsion type at different salinities of the motor oil system with $C_{14-15}(PO)_5SO_4Na$. At low salinities or in the Winsor's type I region, the conductivity increases steadily with salinity. This is because the microemulsion consists of oil droplets dispersed in the aqueous solution which is the continuous phase. In the Winsor's type III region, the system has two continuous

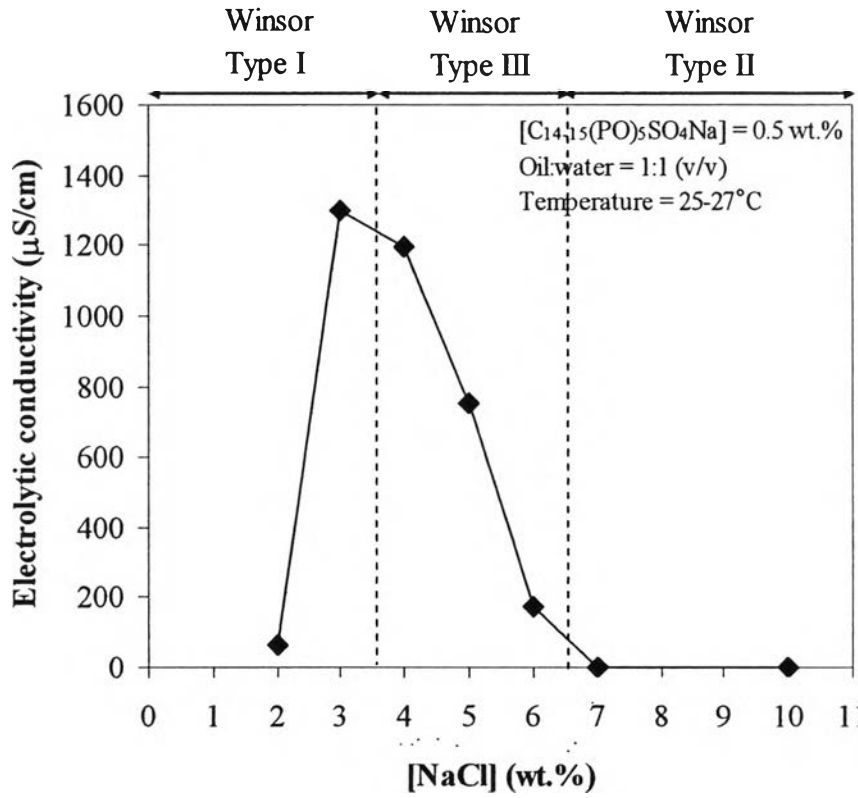

Figure 5.3 Electrolytic conductivity of different microemulsion systems at different NaCl concentration.

phases of motor oil and water, resulting in high conductivity. However, the conductivity decreased with increasing salinity. This is because the brine droplet dispersed in oil phase. A further increase in salinity results in the phase transformation from Winsor's type III to Winsor's type II microemulsions which brine droplets completely disperse in the oil phase, leading to lowering the system conductivity. Figure 5.4 presents the surfactant concentration/salinity phase diagram (fish diagram) showing the regions where different microemulsion types exist for the motor oil/water microemulsion system at an oil-to-water ratio of 1:1. The fish diagram was constructed by using the visual observation at very high surfactant concentrations and the conductivity and IFT data at low surfactant concentrations. The electrical conductivity of the microemulsion was immediately measured, under gentle magnetic stirring. Under these conditions, the obtained value of conductivity remained constant for a long time, and was found to be relatively steady (± 5%). In addition, the IFT of the system was measured by the spinning drop tensiometer to

examine the existence of the Winsor's type III microemulsions. The plots of IFT as a function of surfactant concentration and salinity are not presented here but available elsewhere (35). For a given surfactant concentration in the range of 0.5-5 wt.% in this study, an increase in salinity (known as salt scan) results in a phase transformation from a Winsor's type I to a Type III, then to a Type II microemulsion, as shown in Figure 5.4. For the motor oil system, the CμC of 0.5 wt.% $C_{14-15}(PO)_5SO_4Na$ was found at 5 wt.% salinity. A $C_{14-15}(PO)_5SO_4Na$ concentration of 0.5 wt.% or the CμC was selected as a base condition to run the froth flotation experiments. A minimum surfactant concentration is preferable for froth flotation operation because of cost and environmental reasons.

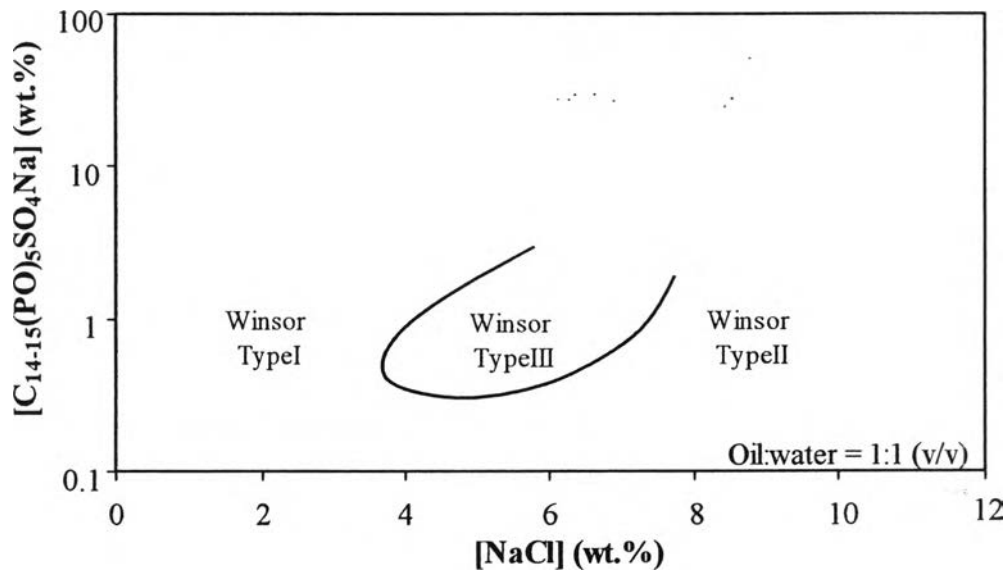

Figure 5.4 Microemulsion phase diagram (Fish diagram) of $C_{14-15}(PO)_5SO_4Na$ as a function of salinity at an oil-to-water ratio of 1:1 and 30°C.

5.4.2 Interfacial Tension (IFT)

Figure 5.5 shows the comparison between the equilibrium IFT and the dynamic IFT at different NaCl concentrations. The equilibrium IFT was measured from the microemulsion sample taken after equilibration. The dynamic IFT measurement was carried out after a fresh motor oil droplet was introduced into the spinning drop tensiometer and starting to extend according to the spinning speed. This simulated condition was referred to the situation when surfactant molecules in the solution to adsorb at the air bubble interfaces in the froth flotation column. The differences between the equilibrium IFT and the dynamic IFT were insignificant, suggesting that the equilibrium IFT can be used to correlate to the process performance of continuous froth flotation. This robust feature of IFT is very useful in the design and operation of a froth flotation unit to treat an oily wastewater without obtaining the equilibrium IFT.

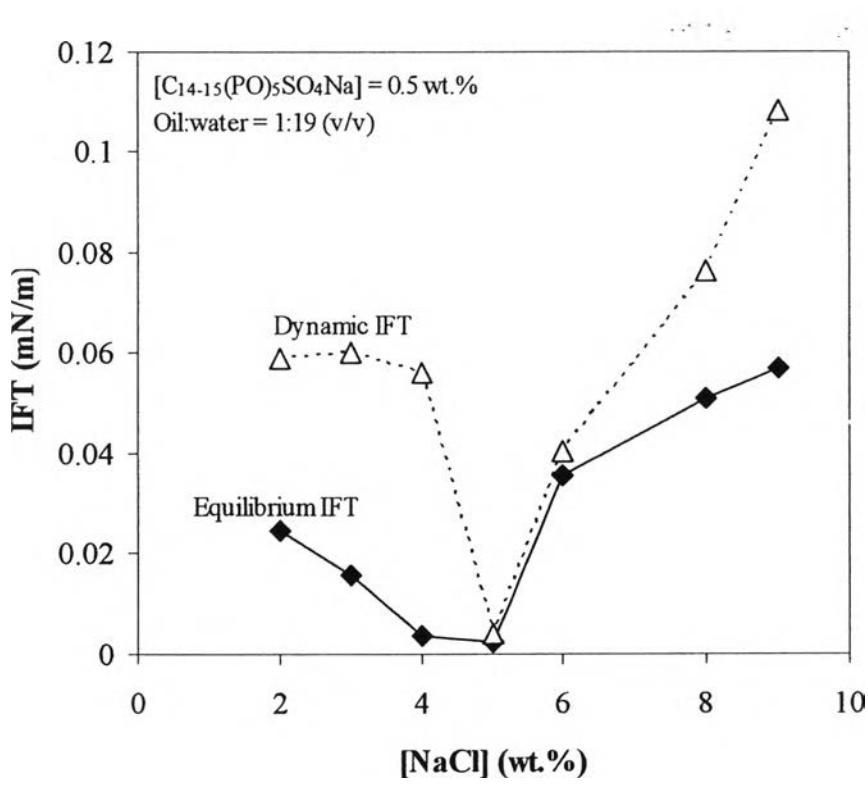

Figure 5.5 Equilibrium IFT and dynamic IFT as a function of salinity at 30°C.

5.4.3 Air Bubble Size Distribution in Froth Flotation Column

A number of studies were conducted to investigate air bubble size in froth flotation columns, ranging from the evaluation of idealized single bubble-single particle systems in laboratory-scale columns, to large-scale industrial flotation units (20, 37-48). The presence of surfactant plays a crucial role affecting the size of the air bubbles in flotation column. The air bubbles are stabilized by the interfacial adsorption of surfactant molecules during the rising step and the coalescence arising from bubble collision is reduced by the repulsive force between the air bubbles (20).

The surfactant adsorption at an air/water interface is the primary mechanism affecting the flotation performance and so it would be expected that the measurement of surface tension should provide a useful basis for the interpretation of surfactant behavior. However, many sub-processes in flotation occur over short periods. Therefore, the interaction of the surfactant with these sub-processes may well occur under conditions where the surface tension is not yet to reach equilibrium. Therefore, the dynamic surface tension becomes more appropriate to aid the interpretation of the process performance of froth flotation process (20).

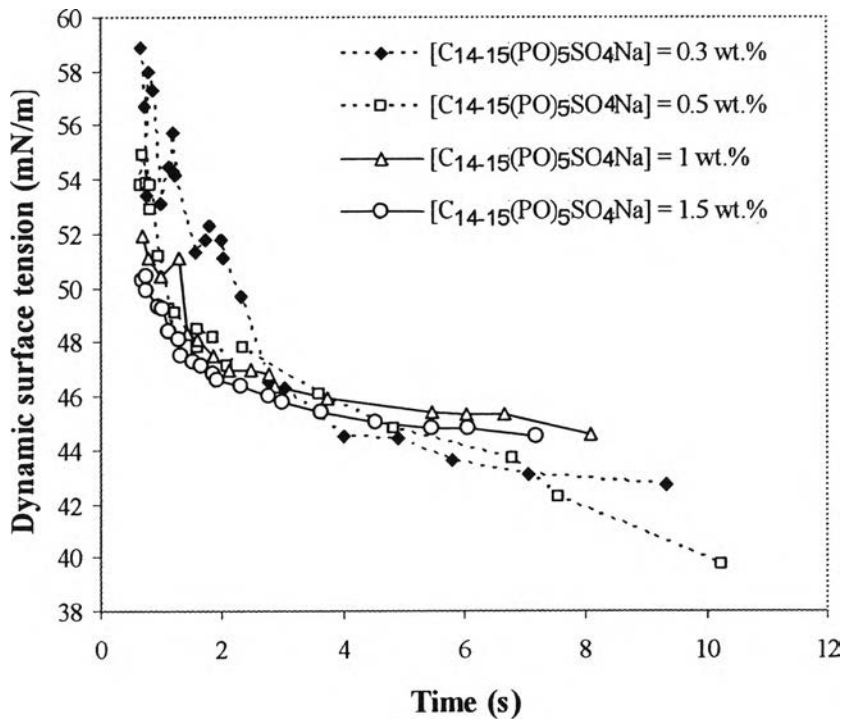

Figure 5.6 Dynamic surface tension of $C_{14\text{-}15}(PO)_5SO_4Na$ solutions at different concentrations, 5 wt.%NaCl, and 30°C.

Figure 5.6 shows the dynamic surface tension of $C_{14\text{-}15}(PO)_5SO_4Na$ solution at different concentrations. The surfactant concentration slightly influenced the dynamic surface tension in the studied range of time and surfactant concentration. It is seen clearly that the lower the surfactant concentration, the longer the time needed to establish the equilibrium value of surface tension (49). From Figure 5.6, the rapid fall of dynamic surface tension shifts to a shorter time with increasing $C_{14\text{-}15}(PO)_5SO_4Na$ concentration. Hence, the value of t^* tended to decrease with the increase in $C_{14\text{-}15}(PO)_5SO_4Na$ concentration.

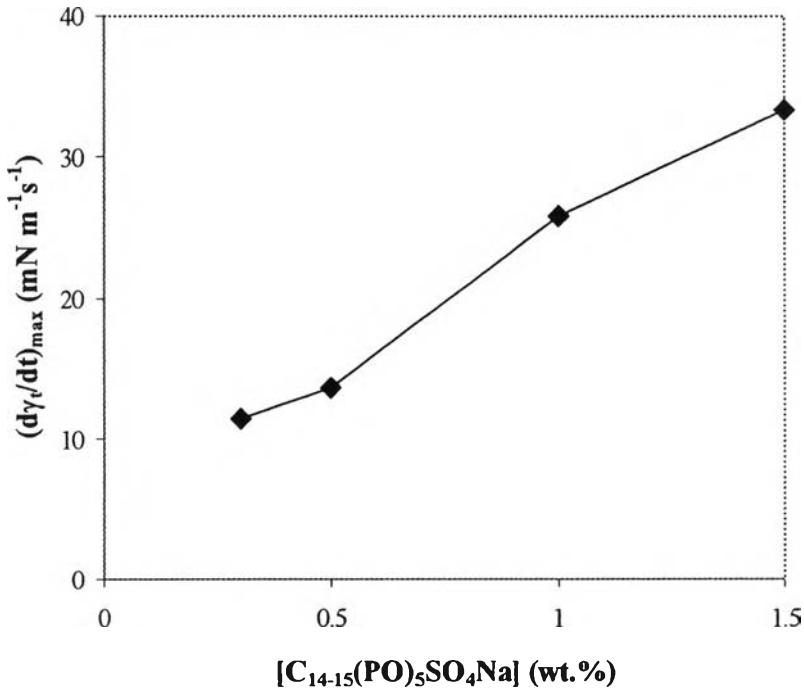

Figure 5.7 Effect of surfactant concentration on $(d\gamma_t/dt)_{max}$.

Figure 5.7 shows the effect of $C_{14\text{-}15}(PO)_5SO_4Na$ concentration on $(d\gamma_t/dt)_{max}$ which represents the dynamic adsorption of the surfactant on the bubbles interface. The fall rate of dynamic surface tension was found to increase almost linearly with increasing $C_{14\text{-}15}(PO)_5SO_4Na$ concentration. The higher the surface tension gradient, the faster the compensation of surface tension at the air-water interfacial region because of the faster movement of surfactant molecules along the interface from a region of low surface tension to one of high surface tension and the

movement of surfactant from the thin-film region into the new-depleted surfactant region (50).

The addition of surfactants can alter the frothing system characteristics and enhance the stability of the froth. Surfactants have the effect of reducing the surface tension of the system, therefore lowering the work required for the initial formation of the froth. Moreover, the presence of surfactant can retard the bubble coalescence owing to the repulsive force between the adsorbed surfactant layers of air bubbles. Consequently, the bubble size decreased with an increase in the surfactant dosage (23, 51-53).

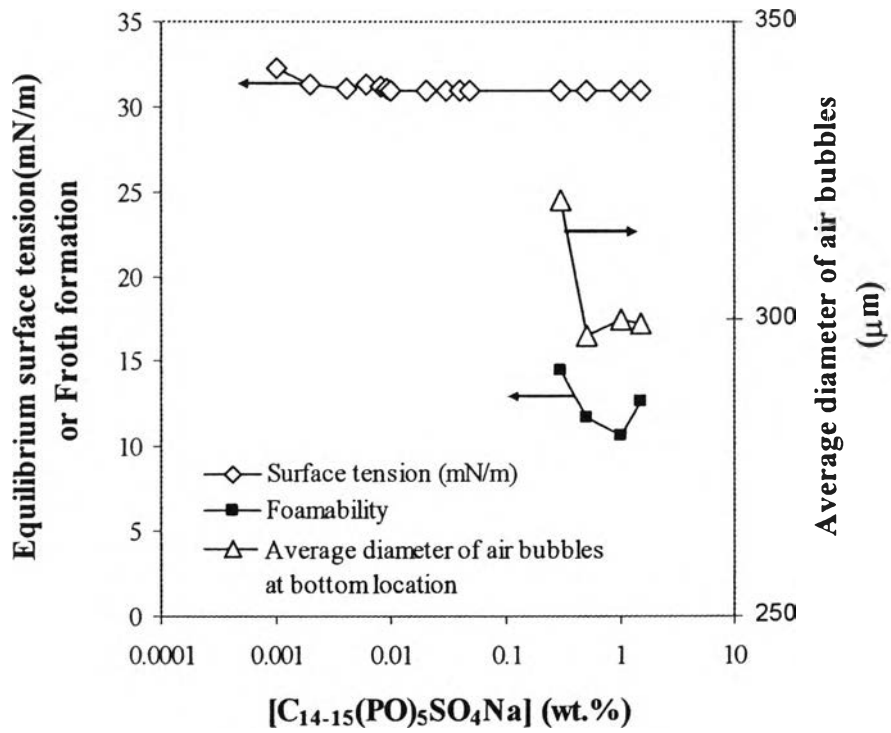

Figure 5.8 Average diameter of air bubbles, equilibrium surface tension, and froth formation at different surfactant concentration.

Figure 5.8 shows the effect of $C_{14\text{-}15}(PO)_5SO_4Na$ concentration on equilibrium surface tension, froth formation, and bubble size. Interestingly, froth formation and average diameter of air bubbles were found to have a similar trend with respect to $C_{14\text{-}15}(PO)_5SO_4Na$ concentrations. Another reason for the limited value of equilibrium surface tension data in the interpretation of flotation frother is the fact that many of the sub-processes in flotation occur over very short time scales (20).

5.4.3.1 Effect of Surfactant Concentration

Figure 5.9 illustrates a comparison of the evolution of air bubble size distribution in flotation column between a surfactant-free system (pure water) (Figure 5.9a) and surfactant systems at different surfactant concentration (Figure 5.9b-5.9e) as a function of axial location of flotation column. It showed that the air bubble size distribution of the surfactant-free system was larger than the air bubble size distribution of the surfactant system due to the effect of surface adsorption. The surfactant adsorption on the air bubble surface reduces the surface tension at the air-water interface, which would consequently reduce the holding forces during bubble formation as well as decrease the coalescence rate of air bubbles as explained before.

(a) Surfactent-free system (pure water)

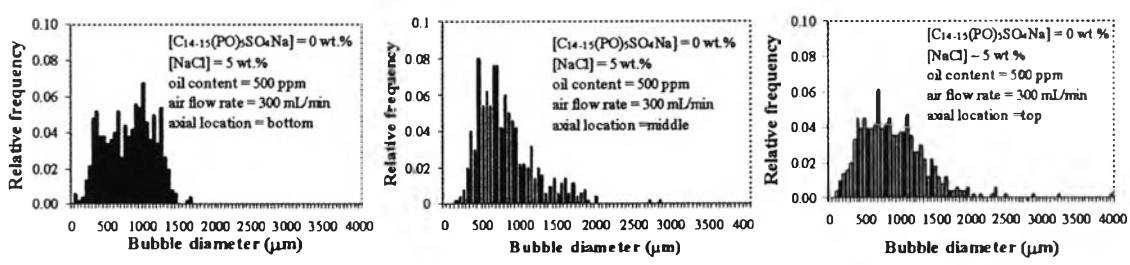

(b) 0.3 wt.% $C_{14\text{-}15}(PO)_5SO_4Na$

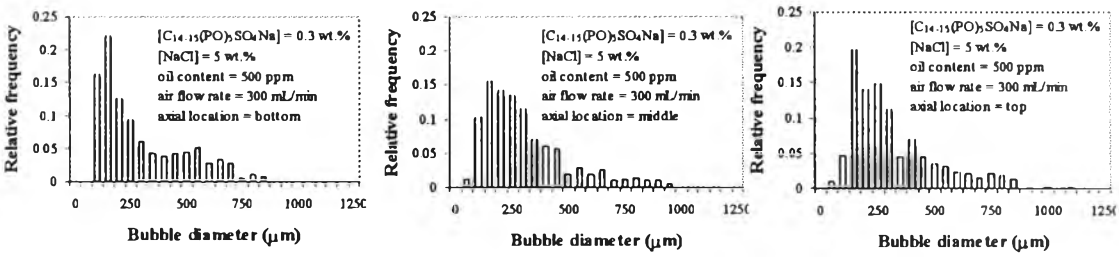

(c) 0.5 wt.% $C_{14\text{-}15}(PO)_5SO_4Na$

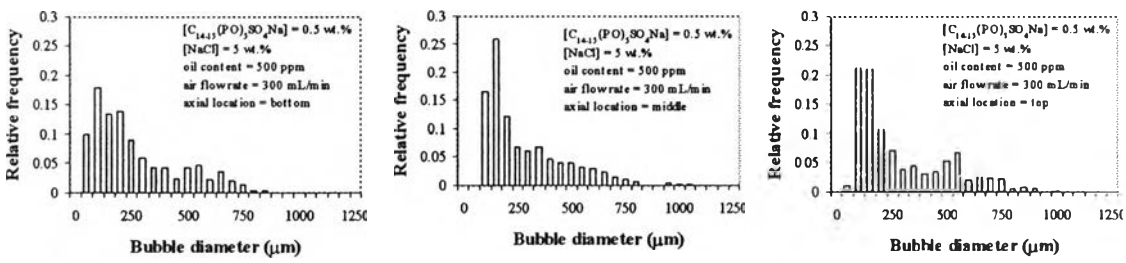

(d) 1 wt.% $C_{14\text{-}15}(PO)_5SO_4Na$

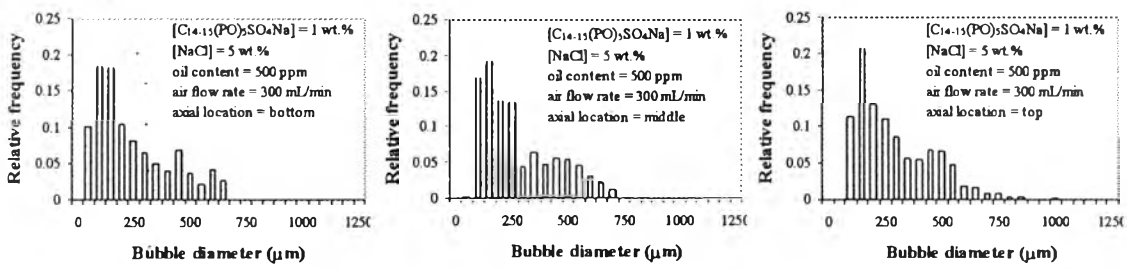

(e) 1.5 wt.% $C_{14\text{-}15}(PO)_5SO_4Na$

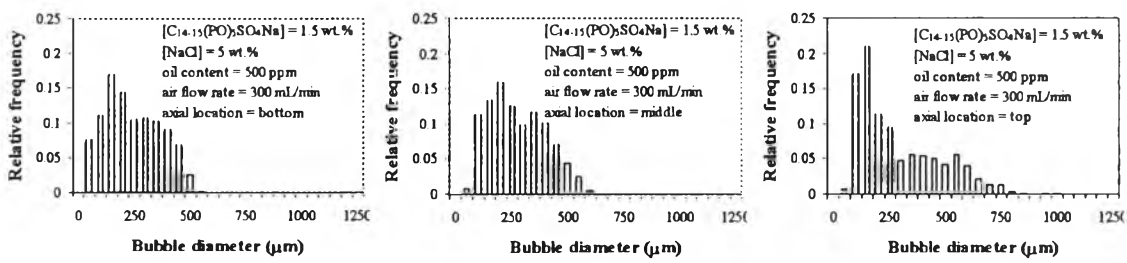

Figure 5.9 The evolution of bubble size distribution in froth flotation column between a surfactant-free system (pure water) and a surfactant system as a function of surfactant concentration and axial location.

In this study, five parameters are used to elucidate the separation performance of froth flotation which are average air bubble size diameter, Sauter mean diameter, air bubble surface area flux, air bubble number flux, and arithmetic mean of specific surface area of air bubbles in a flotation column (54-60). All of these air bubble parameters are needed to be taken into consideration for the scale up of a froth flotation column apart from basic process parameters such as surfactant concentration, hydraulic retention time, etc. For example, different flotation column sizes can provide substantially similar flotation performance when the operating variables are adjusted to meet the same air bubble surface area flux (55).

The average air bubble size diameter, d_{ave}, is defined by Eq. [4];

$$d_{ave} = \sum d_i / \sum N \quad [4]$$

where d_i is diameter of air bubble i (μm), N is a total number of air bubbles (55).

The Sauter mean diameter is also call the d_{32} and is defined as Eq. [5];

$$d_{32} = \sum n d_i^3 / \sum n d_i^2 \quad [5]$$

where d_{32} is Sauter mean diameter (μm), d_i is the equivalent spherical diameter (μm), n is the number of bubbles (56, 57).

The air bubble surface area flux of the air bubbles is defined as the total surface area of air bubbles that rise across a given plane per second devided by the cross-sectional area of the flotation column. The air bubble surface area flux is calculated from the size distribution of air bubbles during the flotation operation. The average air bubble diameter which determined from the bubble size distribution is used to calculate the total surface area of air bubbles crossing the plane per second (54). A higher air bubble surface area flux means a higher possibility for oil to adhere to the air bubbles, which subsequently results in a higher oil removal.

The air bubble number flux, N(Z), is calculated based on the gas volumetric flow rate, Q_g, divided by the cross-sectional area of a froth flotation column and the average volume of air bubbles, A_c. The average volume of air bubbles is calculated from the Sauter mean diameter, d_{32}. The bubble number flux expressed by Eq. [6] (58):

$$N(Z) = \frac{\text{Gas volumetric flow rate}}{\text{Bubble volume x Cross-sectional area}} = \frac{Q_g}{\P/6d^3_{32} \times \P/4d^2_c} = \frac{24Q_g}{d^3_{32} \times d^2_c} \quad [6]$$

The specific surface area of air bubbles is another practical parameter to indicate the froth flotation performance because the separation or the mass transfer occurs on the surface of the rising air bubbles. The larger the specific surface area, the higher the possibility for oil attachment at the air bubble surfaces. The specific surface area of air bubbles is calculated based on the air bubble size distribution data. It defined as the ratio of surface area to volume of bubble as Eq. [7].

$$S_b = \frac{\sum a_i / v_i}{N} \quad [7]$$

where S_b is a arithmatic mean of specific surface area (m^2/m^3), a_i is surface area of bubble i (m^2), v_i is volume of bubble i (m^3) (56).

Figure 5.10 represents a comparison of the air bubble size parameters between the surfactant-free system (pure water) and the surfactant-containing system. The results showed that the presence of surfactant resulted in lowering the average air bubble diameter, and the Sauter mean diameter but increasing the air bubble surface area flux, the air bubble number flux and the specific surface area of air bubbles. The results can be explained in that, the surfactant adsorption at the gas/liquid interface stabilizes the liquid film surrounding a bubble, and to reduce the bubble coalescence. The higher the air bubble surface

area and the specific surface area of air bubbles, the higher the oil attachment on the air bubbles, leading to higher oil removal (20,47). This correlation will be discussed later.

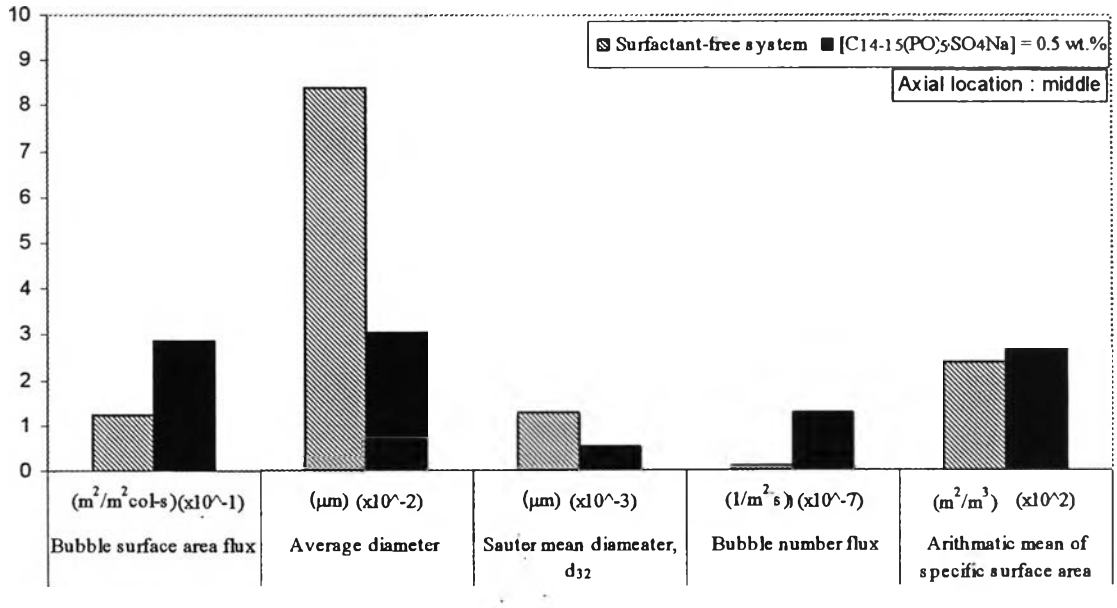

Figure 5.10 Comparison of bubble size parameters between the surfactant-free system (pure water) and surfactant-containing system.

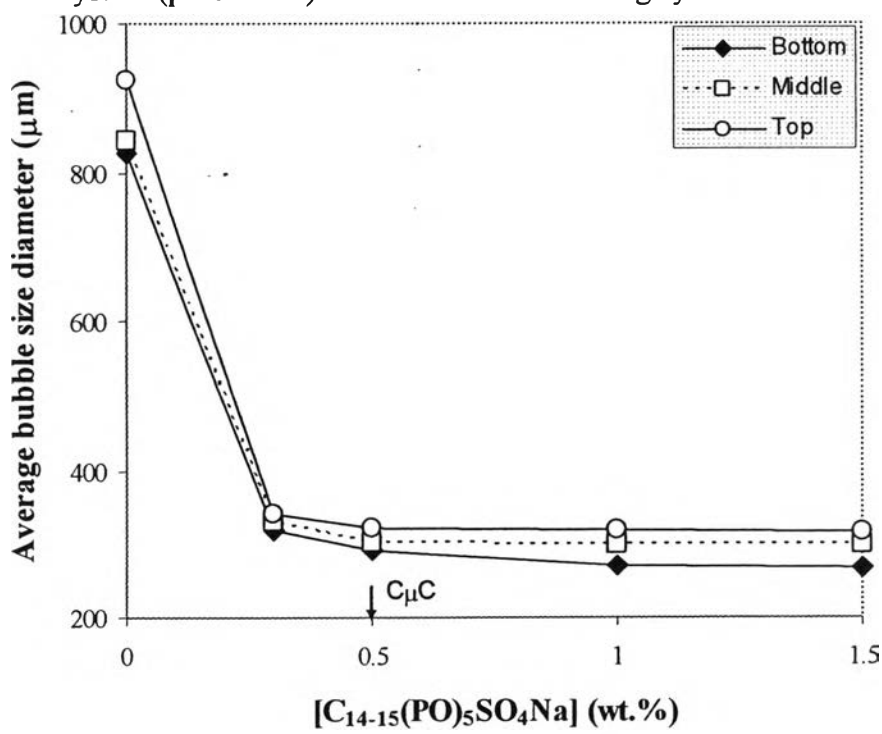

Figure 5.11 Average bubble size diameter as a function of $C_{14\text{-}15}(PO)_5SO_4Na$ concentration at three different axial locations ([motor oil] = 500 ppm; [NaCl] = 5 wt.%; air flow rate = 300 ml/min; and HRT = 30 min).

Interestingly, Figure 11 shows an average bubble size diameter as a function of $C_{14\text{-}15}(PO)_5SO_4Na$ concentration at three different axial locations. For any given axial location, the average bubble size diameter decreased sharply with increasing $C_{14\text{-}15}(PO)_5SO_4Na$ concentration in the range of 0-0.3 wt.%. Beyond the $C_{14\text{-}15}(PO)_5SO_4Na$ concentration of 0.5 wt.% which is the CμC, the average diameter of air bubbles remained almost unchanged with increasing $C_{14\text{-}15}(PO)_5SO_4Na$ concentration. Interestingly, for any given $C_{14\text{-}15}(PO)_5SO_4Na$ concentration, an increase in the liquid height in the froth flotation column increased slightly the average diameter of air bubbles. As well, the trend of the Suater mean diameter as a function of $C_{14\text{-}15}(PO)_5SO_4Na$ concentration at all three different axial locations similar to the average bubble size diameter, with the optimum surfactant concentration of 0.5 wt.%, as shows in Figure 12. The smaller bubble diameter with increasing $C_{14\text{-}15}(PO)_5SO_4Na$ concentration results in the larger specific surface area, as shows in Figure 13 as well as the larger bubble surface area flux, as shows in Figure 14 and the bubble number flux as shows in Figure 15. The bubble number flux is inversely proportional to the Suater mean diameter, as defined in Eq. [6].

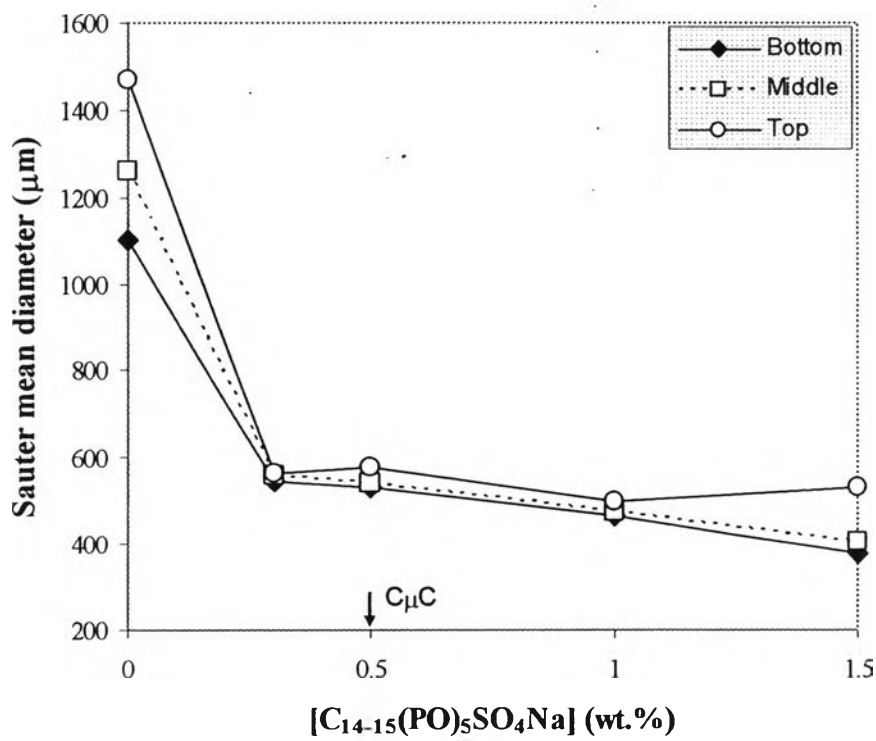

Figure 5.12 Sauter mean diameter as a function of $C_{14\text{-}15}(PO)_5SO_4Na$ concentration at three different axial locations ([motor oil] = 500 ppm; [NaCl] = 5 wt.%; air flow rate = 300 ml/min; and HRT = 30 min).

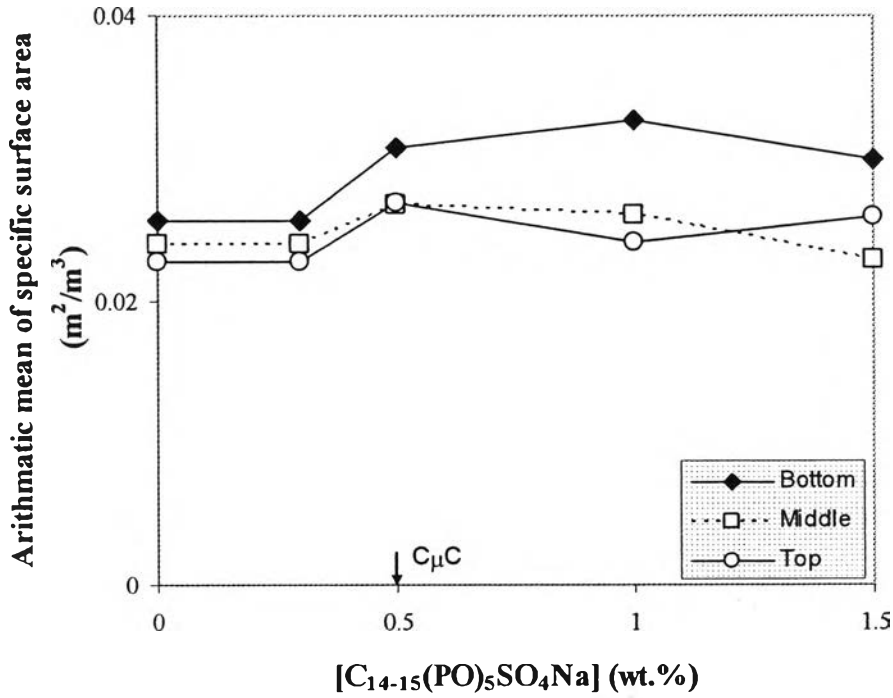

Figure 5.13 The specific surface area as a function of $C_{14\text{-}15}(PO)_5SO_4Na$ concentration at three different axial locations ([motor oil] = 500 ppm; [NaCl] = 5 wt.%; air flow rate = 300 ml/min; and HRT = 30 min).

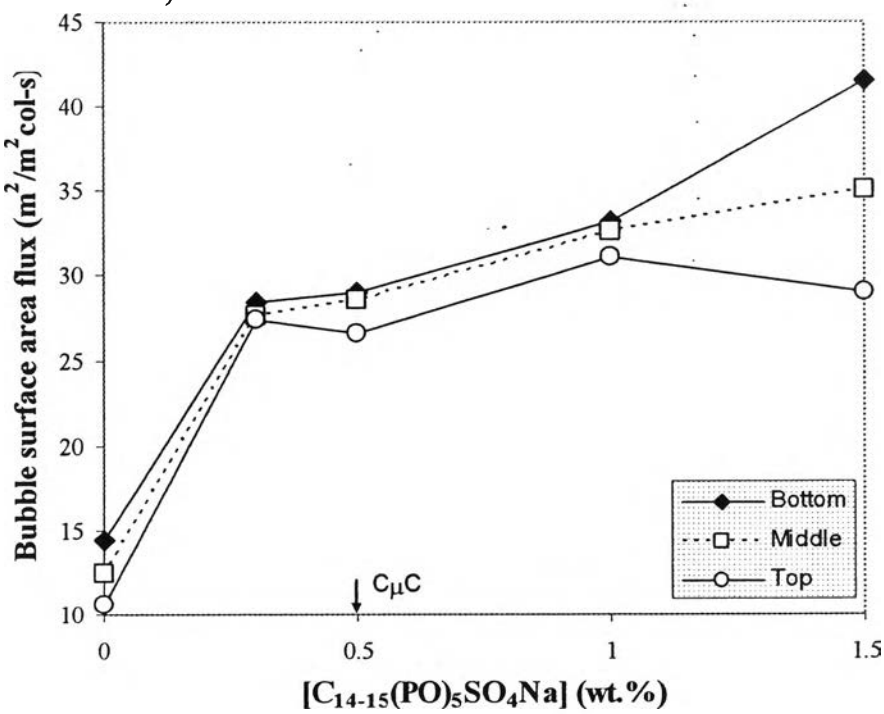

Figure 5.14 Bubble surface area flux as a function of $C_{14\text{-}15}(PO)_5SO_4Na$ concentration at three different axial locations ([motor oil] = 500 ppm; [NaCl] = 5 wt.%; air flow rate = 300 ml/min; and HRT = 30 min).

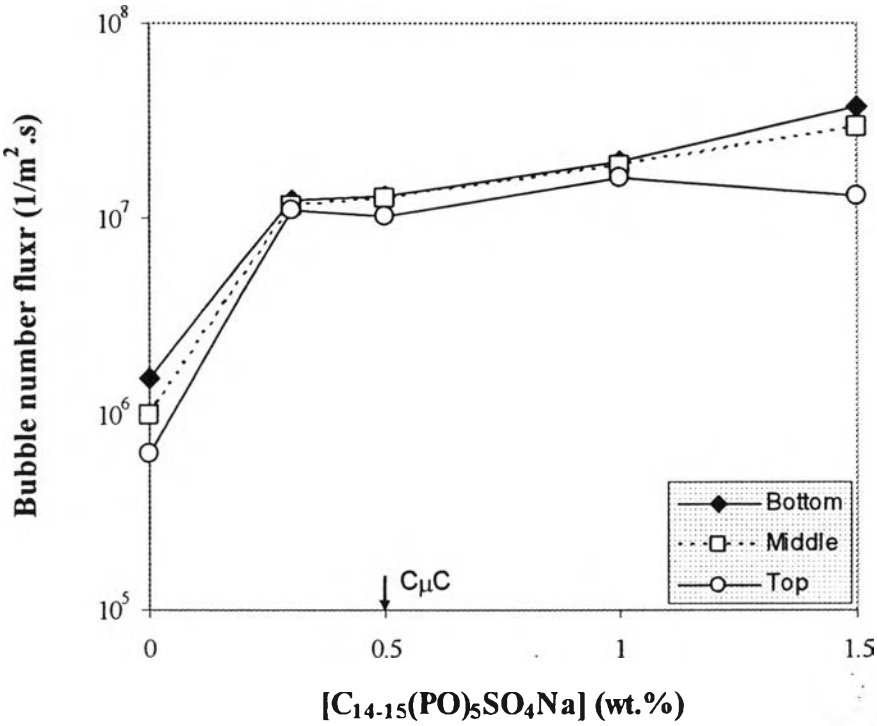

Figure 5.15 Bubble number flux as a function of $C_{14\text{-}15}(PO)_5SO_4Na$ concentration at three different axial locations ([motor oil] = 500 ppm; [NaCl] = 5 wt.%; air flow rate = 300 ml/min; and HRT = 30 min).

5.4.3.2 Effect of Column Height

Figure 5.9 shows the bubble size distribution obtained at three axial positions (bottom, middle and top of the column). The bubble diameter increases with the increase in the distance from the bottom of the column due to the coalescence of smaller bubbles. The coalesced bubbles at the bottom go up due to their buoyancy and accumulate at the middle and the top of the column. In addition, because of the surfactant property as mentioned in the effect of surfactant concentration on the bubble size distribution, the bubbles would not break when they ascend through the top of the column. Figure 5.16 shows effect of axial location of flotation column on bubble size parameters of a surfactant-free system (Figure 5.16a) and a surfactant system

(Figure 5.16b). The results of bubble size parameters in both the surfactant-free system and the surfactant system are in the same trend. According to the coalescence of smaller bubbles, the average bubble size diameter and Suater mean diameter increase with the increase in the distance from the bottom of the column. Consequently, the bubble surface area flux, bubble number flux, and arithmetic mean of specific surface area decrease with increasing of distance of axial location from bottom to top of the column as mentioned before in the effect of surfactant concentration on the bubble size distribution.

a)

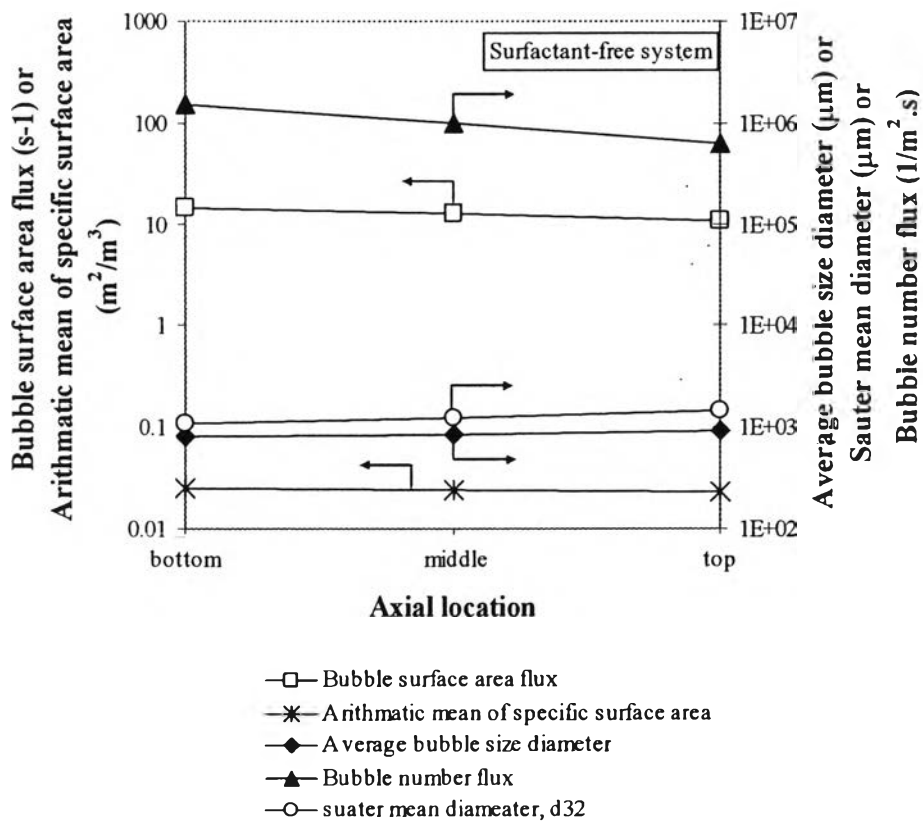

b)

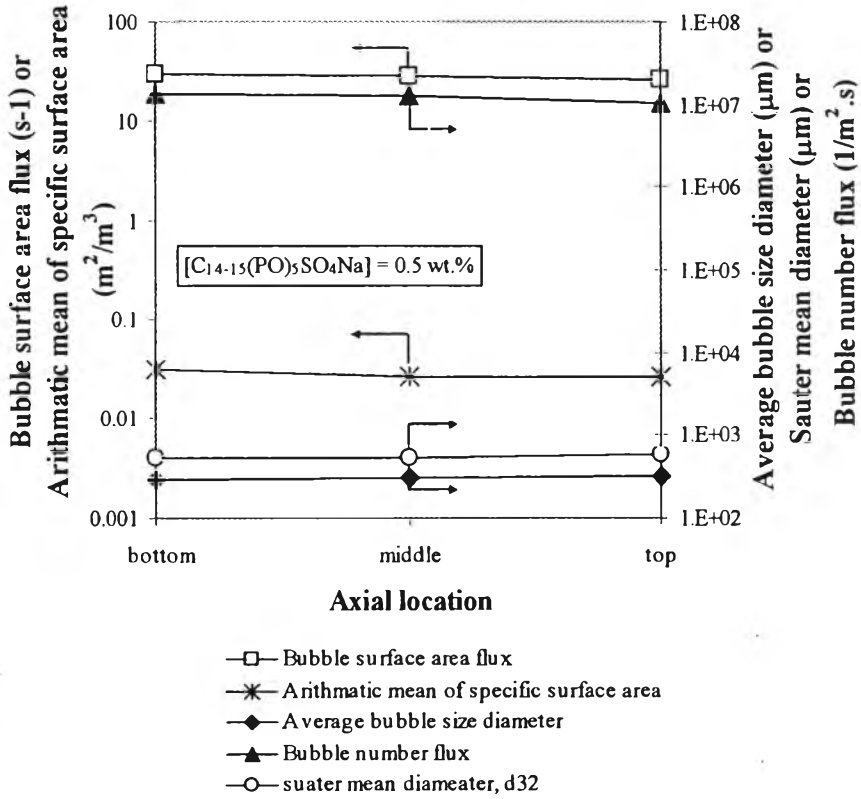

Figure 5.16 Effect of axial location of flotation column on the bubble size parameters at (a) surfactant-free system; (b) 0.5 wt.% of $C_{14\text{-}15}(PO)_5SO_4Na$.

5.4.3.3 Bubble Axial Velocity

Figure 5.17 shows bubble axial velocity distribution as a function of surfactant conentration at bottom location of flotation column. The average bubble axial velocity is calculated from the bubble axial velocity distributions. An increase in $C_{14\text{-}15}(PO)_5SO_4Na$ caused a broader axial velocity distribution of air bubbles. The maximum axial velocity of air bubbles shifted to a lower value with increasing $C_{14\text{-}15}(PO)_5SO_4Na$ concentration.

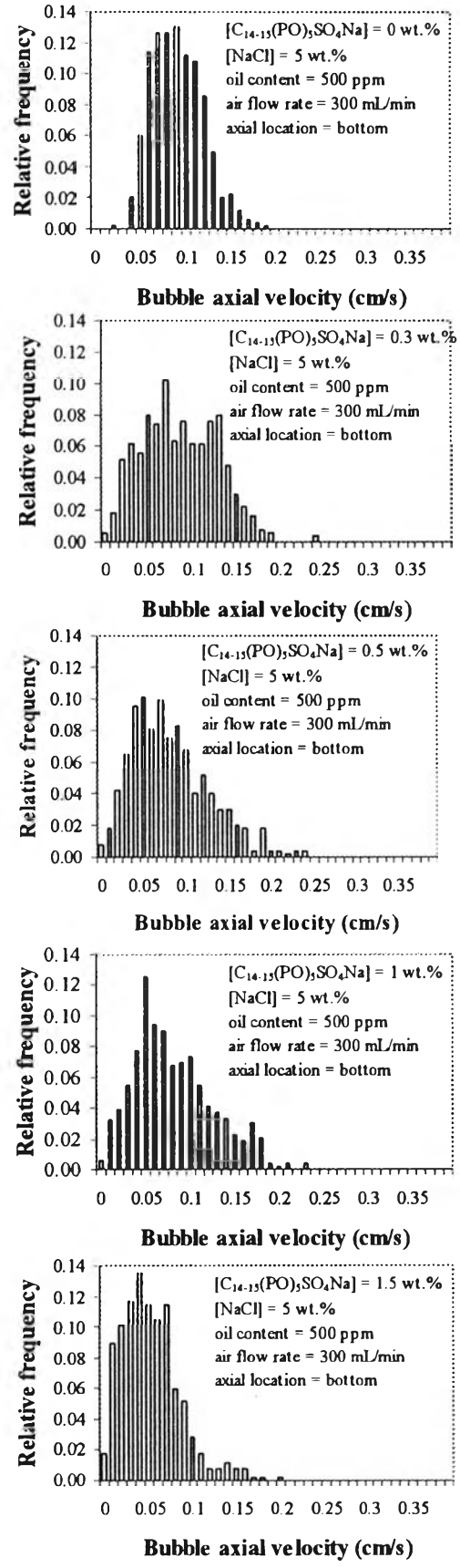

Figure 5.17 Bubble axial velocity distributions as a function of surfactant concentration at bottom location.

Figure 5.18 shows the average axial velocity and the average residence time of air bubbles in the froth flotation column as a function of surfactant concentration with increasing $C_{14\text{-}15}(PO)_5SO_4Na$ concentration, the average axial velocity increased whereas the average residence time of air bubbles decreased. It can be clearly stated that the bubble velocity profile is surfactant concentration dependent (59). From Figure 5.18, as the $C_{14\text{-}15}(PO)_5SO_4Na$ concentration increases resulting in the decreasing of average bubble axial velocity associated with a decrease in bubble size due to the buoyancy force (60). These results correspond with the increase of the air bubble residence time in the froth flotation column. The air bubble residence time was influenced by the amount of surfactant concentration. It was found that the higher surfactant concentration, the longer air bubble residence time in the froth flotation column leading to the higher possibility for air bubble interfaces to contact and was adsorbed with oil droplets.

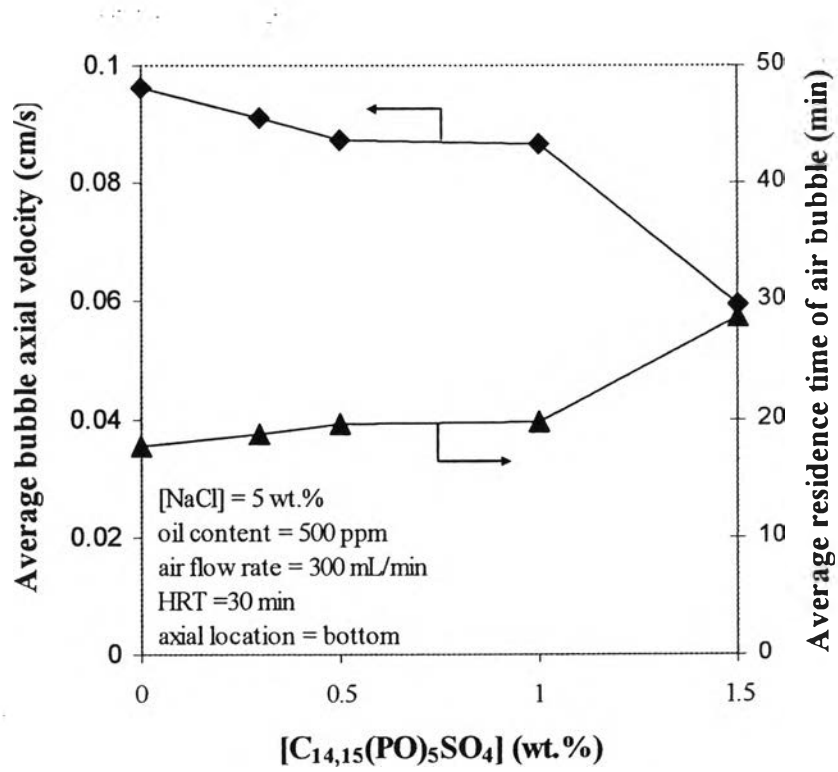

Figure 5.18 Average bubble axial velocity as a function of surfactant.

5.4.4 Froth Flotation Performance

Generally, high oil removal efficiency is a vital requirement for an effective froth flotation operation. If both oil and water are present in the froth with the same proportions as those in the influent, the separation of oil from water does not occur. Hence, for effective separation, the concentration of oil in the overhead froth has to be much higher than that in the feed. Consequently, in this study, both the removal and enrichment ratio of motor oil are used to evaluate the separation efficiency of the studied continuous froth flotation system. Motor oil removal is calculated based on the mass difference of motor oil in the feed and in the effluent. The enrichment ratio of motor oil is defined as the ratio of the concentration of motor oil in the liquid from the overhead froth to that in the feed solution. The higher the enrichment ratio of motor oil, the better the separation efficiency.

5.4.4.1 Effect of Surfactant Concentration

Figure 5.19 shows the effect of surfactant concentration on the process performance of continuous froth flotation operated at 5 wt.% NaCl, an air flow rate of 300ml/min, an oil concentration of 500 ppm and a hydraulic retention time (HRT) of 30 min. The maximum motor oil removal was achieved at 0.5 wt.% $C_{14\text{-}15}(PO)_5SO_4Na$ which is the CμC. The trend of motor oil removal as a function of $C_{14\text{-}15}(PO)_5SO_4Na$ concentration was found to mirror the effect on froth production rate. For the $C_{14\text{-}15}(PO)_5SO_4Na$ concentration in the range of 0.3 to 0.5 wt.%, the oil removal increases because there is more froth to produce with increasing surfactant concentration. Then, the oil removal decreases as the $C_{14\text{-}15}(PO)_5SO_4Na$ concentration increases from 0.5 to 1.0 wt.%. This may be because at higher $C_{14\text{-}15}(PO)_5SO_4Na$ concentration, there is more water in the foam lamellae also known as wet froth. Consequently, froth with higher $C_{14\text{-}15}(PO)_5SO_4Na$ concentration is heavier than that with lower $C_{14\text{-}15}(PO)_5SO_4Na$ concentration leading to the collapse of froth much easier. When the $C_{14\text{-}15}(PO)_5SO_4Na$ concentration further increases to 1.5 wt.%, the oil removal increases again because the rate of froth production increases. Even though the increase in the $C_{14\text{-}15}(PO)_5SO_4Na$ concentration increases the thickness of foam lamella leading to the collapse of the froth, there is more easily to

balance between the ability of the froth formation due to the high concentration of surfactant and the froth collapse due to the wet froth.

As the $C_{14\text{-}15}(PO)_5SO_4Na$ concentration increases from 0.3 wt.% to 0.5 wt.%, the enrichment ratio slightly decreases because the concentration of surfactant at the froth decreases with increasing feed $C_{14\text{-}15}(PO)_5SO_4Na$ concentration. Hence, the foam lamellae with higher surfactant concentration becomes thicker than that with lower surfactant concentration leading to a large amount of water in the foam lamellae, so 0.5 wt.% $C_{14\text{-}15}(PO)_5SO_4Na$ results in the low enrichment ratio of motor oil. However, when the $C_{14\text{-}15}(PO)_5SO_4Na$ concentration further increases, the enrichment ratio slightly increases. This is because increasing surfactant concentration increases the hydrophobic region. Thus, the amount of oil content in the froth increases.

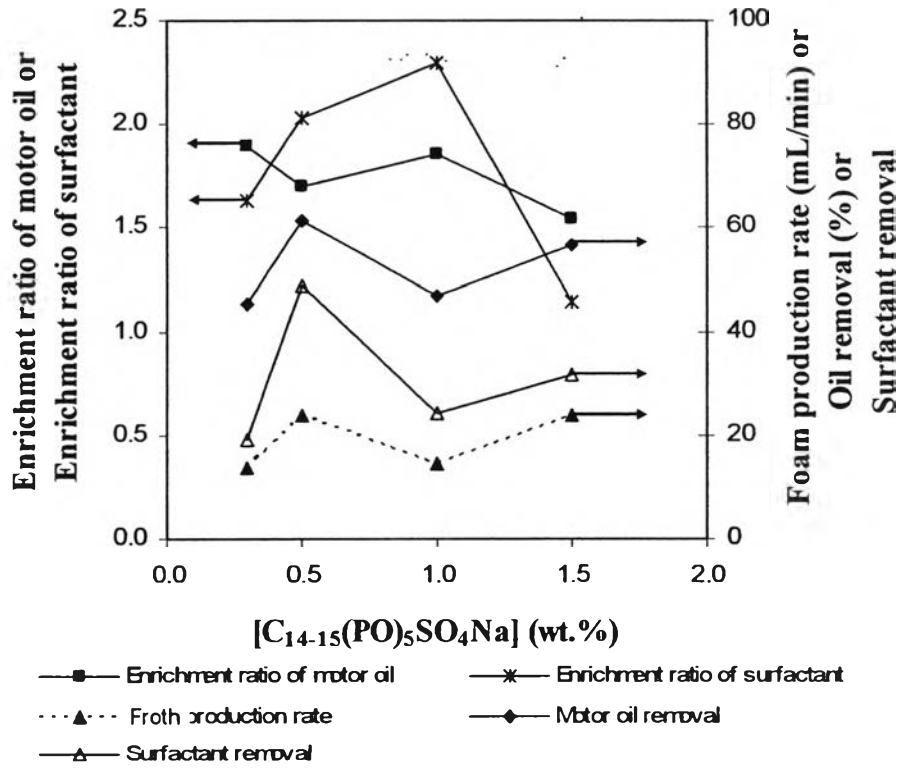

Figure 5.19 Effect of $C_{14\text{-}15}(PO)_5SO_4Na$ concentration on process parameters for continuous froth flotation operated at an air flow rate of 300 ml/min, a HRT of 30 min, a NaCl concentration of 5 wt.%, and an oil concentration of 500 ppm.

When considering the bubble size diameter (Figure 5.11), it was found that at surfactant concentration 0.3 wt%, the average bubble size diameter is higher than the other condition. Therefore, it leads to the lower oil removal because of increasing in bubble size diameter resulting in the decrease in the specific area of gas-liquid interface that cause the low possibility for the oil adsorption while other three concentration of surfactant have the average bubble size diameter in the same range. Hence, it doesn't affect too much on the oil removal efficiency. In terms of the average bubble axial velocity results (Figure 5.18), the bubble axial velocity decrease with increasing of surfactant concentration results in longer residence time of bubbles in the flotation column to encounter with oil droplets. Therefore, at high surfactant concentrations seems to be a suitable condition for the froth flotation performance. However, the froth characteristics play a more significant role than the bubble size characteristics and the average bubble axial velocity on the oil removal performance because the motor oil removal has the same trend as froth production rate as it was revealed in the previous work (11, 12).

5.4.4.2 Effect of Hydraulic Retention Time (HRT)

The term of hydraulic retention time (HRT) is expressed as the holding or residence time of the liquid in the froth flotation column which is calculated from the liquid volume in the column divided by the feed flow rate. Figure 5.20 shows the effect of HRT on all process parameters of the continuous froth flotation unit operated under the base conditions. The motor oil removal decreases when HRT increases. Even though a higher HRT represents a longer residence time of motor oil in the flotation column to be adsorbed onto and coalesced with the rising air bubbles interface, a lower amount of surfactant can be carried into the column resulted in lower froth to produce with increasing HRT. In this study, the highest motor oil removal (61.5%) is achieved at 30 min HRT.

As the HRT increases from 30 min to 45 min, the enrichment ratio slightly increases. This is because a high HRT represents a lower feed flow rate resulting in more time of oil stay in the column as well as more time to be contacted and attached to the air bubbles and the froth at the top of the column. Therefore, in the collapsed froth contains a higher amount of oil and smaller water content with

increasing HRT. However, when the HRT further increases, the enrichment ratio decreases. This may be because an increase in the HRT corresponds to a longer time for the froth rises to the top of the column leading to collapse of the froth. A similar trend of the enrichment ratio of surfactant was found in the studied range of HRT. This reason can be explained as described in the effect of HRT on the enrichment ratio of motor oil.

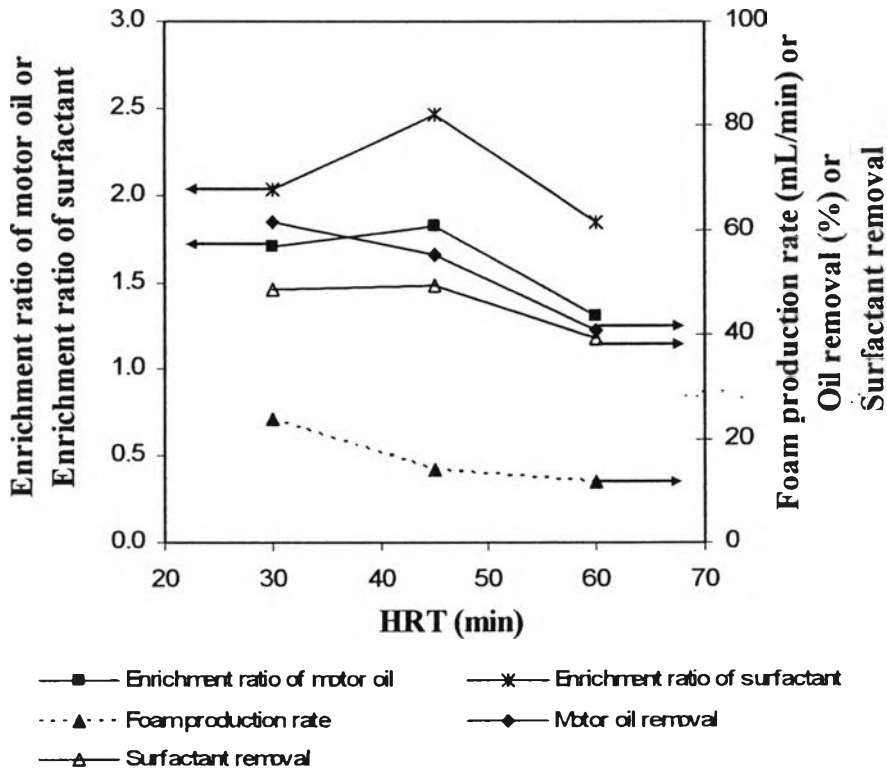

Figure 5.20 Effect of HRT on process parameters for continuous froth flotation.

5.5 Acknowledgements

The Thailand Research Fund is acknowledged for providing a Royal Golden Jubilee Ph.D. fellowship for Ms. Sunisa Watcharasing. The expenses for this research were mainly supported by The Advanced Research Scholar Grant from The Thailand Research Fund and The Research Unit of Applied Surfactants for Separation and Pollution Control under The Ratchadapisek Somphot Fund, Chulalongkorn University. The National Excellence Center for Petroleum, Petrochemicals and Advanced

Materials under The Ministry of Education is also acknowledged for providing all research facilities. Sasol North America Inc., Texas, USA, is acknowledged for providing the extended surfactant used in this research.

5.6 References

1. Mortier, R.M.; Orszulik, S.T. (2000) *Chemistry and Technology of Lubricants*; Great Britain: St Edmundsbury.

2. Fuerstenau, D.W.; Herrera-Urbina, R. (1989) Mineral Separation by Froth Flotation. In: *Surfactant Based Separation Processes*; Scamehorn, J.F.; Harwell, J.H., eds.; Marcel Dekker: New York, 259-320.

3. Somasundaran, P.; Ananthapadmanabhan, K.P. (1987) Bubble and Foam Separations-Ore Flotation, In: *Handbook of Separation Process Technology*; Rousseau, R.W., ed.; Wiley: New York, 775-805.

4. Scamehorn, J.F.; Sabatini, D.A.; Harwell, J.H. (2004) Surfactants, Part II: Applications, In: *Encyclopedia of Supramolecular Chemistry*, Atwood, J.L.; Steed, J.W. eds.; Marcel Dekker: New York; Vol. 1, 1470-1477.

5. Yorar, B. (1997) Flotation, In: *Encyclopedia of Separation Technology*; Ruthven, D.M., ed.; Wiley: New York; Vol. 2, 913-939.

6. Aplan, F.F. (1997) Flotation. In: *Handbook of Separation Techniques for Chemical Engineering*; 3rd Ed.; Schweitzer, P.A., ed.; McGraw-Hill: New York, 5-33-5-42.

7. Pondstabodee, S.; Scamehorn, J.F.; Chavadej, S.; Harwell, J.H. (1998) Removal of ortho-dichlorobenzene by froth flotation under Winsor's type III conditions. *Sep. Sci. Technol.*, *33*: 591-609.

8. Chavadej, S.; Phoochinda, W.; Yanatatsaneejit, U.; Scamehorn, J.F. (2004) Clean-up of oily wastewater by froth flotation: Effect of microemulsion formation III: Use of anionic/nonionic surfactant mixtures and effect of relative volumes of dissimilar phases. *Sep. Sci. Technol.*, *39*: 3097-3112.

9. Yanatatsaneejit, U.; Witthayapanyanon, A.; Rangsunvigit, P.; Acosta, E.J.; Sabatini, D.A.; Scamehorn, J.F.; Chavadej, S. (2005) Ethylbenzene removal by froth flotation under conditions of middle-phase microemulsion formation I: Interfacial tension, foamability, and foam stability. *Sep. Sci. Technol.*, *40*: 1537-1553.

10. Yanatatsaneejit, U.; Chavadej, S; Rangsunvigit, P.; Scamehorn, J.F. (2005) Ethylbenzene removal by froth flotation under conditions of middle-phase microemulsion formation II: Effect of air flow rate, oil-to-water ratio, and equilibration time. *Sep. Sci. Technol.*, *40*: 1609-1620.

11. Yanatatsaneejit, U.; Rangsunvigit, P.; Scamehorn, J.F.; Chavadej, S. (2008) Diesel oil removal by froth flotation under low interfacial tension conditions I: Foam characteristics and equilibration time. *Sep. Sci. Technol.*, *43*: 1520-1534.

12. Watcharasing, S.; Chavadej. S.; Scamehorn, J.F. Diesel oil removal by froth flotation under low interfacial tension conditions II: Continuous mode of operation. Accepted to Sep. Sci. Technol.

13. Choi, S.J.; Choi, Y.H. (1996) Removal of direct red from aqueous solution by foam separation techniques of ion and adsorbing colloid flotation. *Sep. Sci. and Technol.*, *31*: 2105-2116.

14. Freund, J.; Dobias, B. (1995) The Role of Surface Tension. In *Flotation Science and Engineer*; Matis, K.A., ed.; Marcel Dekker, Inc.: New York, 45-61.

15. Bourrel, M.; Schechter, R.S. (1988) *Microemulsion and Related Systems*; Marcel Dekker, Inc.: New York, 127-205.

16. Carre, B.; Fabry, B.; Beneventi, D. (2002) Interfacial mechanisms in deinking process. *Prog. Pap. Recycling.*, *11*: 6-16.

17. Polli, M.; Stanislao, M.D.; Bagatin, R.; Bakr, E.A., Masi, M. (2002) Bubble size distribution in the sparger region of bubble columns. *Chem. Eng. Sci.*, *57*: 197-205.

18. García-Salas, S; Rosales Peña Alfaroa, M.E.; Porterc, R.M.; Thalasso, F. (2008) Masurement of local specific interfacial area in bubble columns via a non-isokinetic withdrawal method coupled to electro-optical detector. *Chem. Eng. Sci.*, *63*: 1029-1038.

19. Majumder, S.K.; Kundu, G., Mukherjee, D. (2006) Bubble size distribution and gas–liquid interfacial area in a modified downflow bubble column. *Chem. Eng. J.*, *122*: 1 – 10.

20. Comley, B.A.; Harris, P.J.; Bradshaw, D.J.; Harris, M.C. (2002) Frother characterisation using dynamic surface tension measurements. *Int. J. Miner. Process.*, *64*: 81-100.

21. Hua, X.Y.; Rosen M.J. (1988) Dynamic surface tension of aqueous surfactant solutions: I. Basic paremeters. *J. Colloid Interface Sci.*, *124*: 652-659.

22. Rodrigue, D.; De Kee, D.; Chan Man Fong, C.F. (1996) An experimental study of the effect of surfactants on the free rise velocity of gas bubbles. *J. Non-Newtonian Fluid Mech.*, *66*: 213-232.

23. Lefebvre, S.; Guy, C. (1999) Characterization of bubble column hydrodynamics with local measurements. *Chem. Eng. Sci.*, *54*: 4895-4902.

24. Irwin, R.J.; VanMouwerik, M.; Stevens, L.; Seese, M.D.; and Basham, W. (1997). Environmental Contaminants Encyclopedia. National Park Service, Water Resources Division, Fort Collins, Colorado.

25. Salager, J.L. (2000) Emulsion Properties and Related Know-how to Attain Them. In *Pharmaceutical Emulsions and Suspensions*; Nielloud, F., Marti-Mestres, G., eds; Marcel Dekker: New York, 73-125.

26. Salager, J.L.; Loaiza-Maldonado, I.; Minana-Perez, M.; Silva F. (1982) Surfactant-oil-water systems near the affinity inversion part I: relationship between equilibrium phase behavior and emulsion type and stability. *J. Dispersion Sci. Technol.*, *3*: 279-292.

27. Rosen, M.J.; Hua, X.Y.; Zhu, Z.H. (1991) In *Surfactants in Solution Vol.* 11; K.L. Mittal and D.O. Shah, eds; Plenum Press: New York, 315.

28. Koval'chuck, V.; Dukhin, S.; Makievski, A.; Fainerman, V.; Miller, R. (1998) Simultaneous calculation of lifetime and deadtime in the maximum bubble pressure measurements. *J. Colloid Interface Sci.*, *198*: 191–200.

29. Tamura, T.; Kaneko, Y.; Ohyama, M. (1995) Dynamic surface tension and foaming properties of aqueous polyoxyethylene n-dodecyl ether solutions. *J. Colloid Interface Sci.*, *173*: 493-499.

30. Colella, D.; Vinci, D.; Bagatin, R.; Masi, M.; Bakr, E.A. (1999) A study on coalescence and breakage mechanisms in three different bubble columns. *Chem. Eng. Sci.*, *54*: 4767-4777.

31. Feng, D.; Aldrich, C. (2000) Removal of diesel from aqueous emulsions by flotation. *Sep. Sci. Technol.*, *35*: 2159-2172.

32. ASTM D1681-92. Standard Test Method for Synthetic Anionic Active Ingredient in Detergents by Cationic Titration Procedure.

33. Perez, M.M.; Graciaa, A.; Lachaise, J.; Salager, J.L. (1995) Solubilization of polar oils with extended surfactants. *Coll. Surf. A.*, *100*: 217-224.

34. Acosta, E., Harwell, J.H., Sabatini, D.A. (2004) Self-assembly in Linker Modified Microemusions. *J. Colloid Interface Sci.*, *274*: 652-664.

35. Kongkowit, W. (2007) Motor Oil Removal from Wastewater by Continuous Froth Flotation. MS thesis. The Petroleum and Petrochemical College, Chulalongkorn University.

36. Rosen, M.J. (2004) *Surfactants and Interfacial Phenomena*, 3rd ed.; Wiley-Interscience: Hoboken, N.J., 277-302.

37. Gorain, B.K.; Franzdis, J.P.; Manlapig, E.V. (1997) Studies on impeller type, impeller speed and air flow rate in an industrial scale flotation cell. part 4: Effect of bubble surface area flux on flotation performance. *Miner. Eng.*, *10*: 367-379.

38. Gorain, B.K.; Franzdis, J.P. ; Manlapig, E.V. (1999) The empirical prediction of bubble surface area flux in mechanical flotation cells from cell design and operating data. *Miner. Eng.*, *12*: 309-322.

39. Finch, J.A.; Xiao, J.; Hardie, C.; Gomez, C.O. (2000) Gas dispersion properties: bubble surface area flux and gas holdup. *Miner. Eng.*, *13*: 365-372.

40. Hu, B; Yang, H.; Hewitt, G.F. (2007) Measurement of bubble size distribution using a flying optical probe technique: Application in the highly turbulent region above a distillation plate. *Chem. Eng. Sci.*, *62*: 2652-2662.

41. Grau, R.A.; Heiskanen K. (2005) Bubble size distribution in laboratory scale flotation cells. *Miner. Eng.*, *18*: 1164–1172.

42. Manera, A.; Prasser, H.-M.; Lucas, D.; Van der Hagen, T.H.J.J. (2006) Three-dimensional flow pattern visualization and bubble size distributions in stationary and transient upward flashing flow. *Int. J. Multiphase Flow*, *32*: 996-1016.

43. Bordel, S.; Mato, R; Villaverde, S. (2006) Modeling of the evolution with length of bubble size distributions in bubble columns. *Chem. Eng. Sci.*, *61*: 3663-3673.

44. Majumder, S.K.; Kundu, G.; Mukherjee, D. (2006) Bubble size distribution and gas–liquid interfacial area in a modified downflow bubble column. *Chem. Eng. J.*, *122*: 1-10.

45. Schäfer, R.; Merten, C.; Eigenberger G. (2002) Bubble size distributions in a bubble column reactor under industrial conditions. *Exp. Therm Fluid Sci.*, *26*: 595-604.

46. Al-Masry, W.A.; Ali, E.M., Aqeel, Y.M. (2006) Effect of antifoam agents on bubble characteristics in bubble columns based on acoustic sound measurements. *Chem. Eng. Sci.*, *61*: 3610-3622.

47. Nguyen, A.V.; Phan, C.M.; Evans, G.M. (2006) Effect of the bubble size on the dynamic adsorption of frothers and collectors in flotation. *Int. J. Miner. Process.*, *79*: 18– 26.

48. Pollia, M.; Stanislaoa, M.D.; Bagatinb, R.; Bakra, E.A.; Masic, M. (2002) Bubble size distribution in the sparger region of bubble columns. *Chem. Eng. Sci.*, *57*: 197-205.

49. Rao, S.R.; Leja, J. (2004) *Surface Chemistry of Froth Flotation Volume1: Fundamentals*; 2nd Ed.; Kluwer Academic/ Plenum Publishers: New York, 143-207.

50. Schramm, L.L.; Wassmuth, F. (1994) Foams: Basic Principles, In *Foam: Fundamentals and Applications in the Petroleum Industry*; Rousseau, Schramm L.L., ed.; American Chemical Society: Washington, DC, 3-46.

51. Aldrich, C.; Feng, D. (2000) The effect of frothers on bubble size distributions in flotation pulp phases and surface froths. *Miner. Eng.*, *13*: 1049-1057.

52. Tucker, J.P.; Deglon, D.A.; Franzidis, J.-P.; Harris, M.; O'Connor, C. (1994) An evaluation of a direct method of bubble size distribution in a laboratory flotation cell. *Miner. Eng.*, *7*: 667–680.

53. Cho, Y.S.; Laskowski, J.S. (2002) Effect of flotation frothers on bubble size and foam stability. *Int. J. Miner. Process.*, *64*: 69–80.

54. Chungchamroenkit, P; Chavadej, S.; Yanatatsaneejit, U.; Kitiyanan, B.; Scamehorn, J.F. Separation of carbon black from silica by froth flotation part I: Effect of operational parameters. Sep. Purif. Technol., *60*: 206–214.

55. Newell, R.; Grano, S. (2007) Hydrodynamics and scale up in rushton turbine flotation cells: Part 1 — cell hydrodynamics. *Int. J. Miner. Process.*, *81*: 224–236.

56. Ventura-Medina, E.; Cillers, J.J. (2000) Calculation of the specific surface area in flotation. *Miner. Eng.*, *13*: 265-275.

57. Garcia-Salasa, S.; Rosales Peña Alfaroa, M.E.; Porterc, R. M; Thalassob F. (2008) Measurement of local specific interfacial area in bubble columns via a non-isokinetic withdrawal method coupled to electro-optical detector. *Chem. Eng. Sci.*, *63*: 1029-1038.

58. Majumder, S.K.; Kundu, G.; Mukherjee, D. (2006) Bubble size distribution and gas–liquid interfacial area in a modified downflow bubble column. *Chem. Eng. J.*, *122*: 1-10.

59. Zhang, Y.; McLaughlinb, J. B.; Finch, J. A. (2001) Bubble velocity profile and model of surfactant mass transfer to bubble surface. *Chem. Eng. Sci.*, *56*: 6605-6616.

60. Azgomi, F.; Gomez, C.O.; Finch, J.A. (2007) Correspondence of gas holdup and bubble size in presence of different frothers. *Int. J. Miner. Process.*, *83*: 1–11.